Review article

Riccardo Degl'Innocenti*, Stephen J. Kindness, Harvey E. Beere and David A. Ritchie

All-integrated terahertz modulators

https://doi.org/10.1515/nanoph-2017-0040
Received April 3, 2017; revised June 15, 2017; accepted June 19, 2017

Abstract: Terahertz (0.1–10 THz corresponding to vacuum wavelengths between 30 μm and 3 mm) research has experienced impressive progress in the last few decades. The importance of this frequency range stems from unique applications in several fields, including spectroscopy, communications, and imaging. THz emitters have experienced great development recently with the advent of the quantum cascade laser, the improvement in the frequency range covered by electronic-based sources, and the increased performance and versatility of time domain spectroscopic systems based on full-spectrum lasers. However, the lack of suitable active optoelectronic devices has hindered the ability of THz technologies to fulfill their potential. The high demand for fast, efficient integrated optical components, such as amplitude, frequency, and polarization modulators, is driving one of the most challenging research areas in photonics. This is partly due to the inherent difficulties in using conventional integrated modulation techniques. This article aims to provide an overview of the different approaches and techniques recently employed in order to overcome this bottleneck.

Keywords: terahertz modulators; metamaterials; integrated optics; 2D materials.

1 Introduction

The terahertz (THz) frequency range, broadly defined between 0.1 and 10 THz, lies in the mm and sub-mm wavelength range of the spectral region. Despite the huge potential offered by this portion of the electromagnetic spectrum, it has been historically neglected and only recently has it experienced a rapid and exponential interest in several research areas. The reasons for this late blooming arise from the intrinsic difficulty of operating in the so-called THz gap [1, 2], lying between the electronic and the photonic range, rather than the lack of scientific applications and fields of investigation. The increasing efforts in THz science and technology are driven by many fields where this radiation finds applications, mainly in communications, spectroscopy, and imaging. Recently, the impressive development in both sources and detectors has been of paramount importance for the progress of this research area. An example of an emitter above 1.5 THz from the electronic side is the uni-travelling carrier photodiode (UTC-PD) source based on III–V semiconductor technology [3, 4], which is directly linked to lasers emitting in the optical communication window. Another important step in the THz source was the advent of quantum cascade laser (QCL) sources [5] and combs [6] either directly engineered to emit in the THz or through the nonlinear processes of mid-infrared QCLs [7–9]. The continuous development of more efficient, integrated, stable, and economic femtosecond (fs) laser sources has greatly improved the state of the art of time domain spectroscopic (TDS) systems. The research into THz detectors has benefited from significant progress in recent years, from GaAs Schottky barrier diodes [10] to the development of detectors based on novel materials, such as graphene [11–15]. The evolution of the basic building blocks for an efficient, integrated THz circuitry has not progressed at the same rapid rate, due to the poor electromagnetic response of naturally occurring materials in this range. In fact, electrical tuning of semiconductor materials proves to be difficult due to the limited change of induced free carrier density, as the photon energies in this range are not sufficient to induce interband absorption. When approaching this range from the microwave side, instead, the free electron response to radiation is limited by several factors, such as the increased absorption at high frequencies, the characteristic transit distance related to the devices' length, and the saturation velocity of electrons. From the electro-optic point of view, there are a few crystals, such as ZnTe or GaP, which are commonly used, for example, for detection in a balanced photodetector scheme, with electro-optic coefficients as high as a few pm/V. However, building a classical integrated device such as a phase or an amplitude modulator [16, 17] would

***Corresponding author: Riccardo Degl'Innocenti,** Department of Physics, University of Cambridge, 19 J J Thomson Avenue, Cambridge CB3 0HE, UK, e-mail: rd448@cam.ac.uk
Stephen J. Kindness, Harvey E. Beere and David A. Ritchie: Department of Physics, University of Cambridge, 19 J J Thomson Avenue, Cambridge CB3 0HE, UK

require prohibitively thick crystals, or the non-trivial implementation of efficient THz waveguides, and operation at high voltages. The lack of active THz optoelectronic components, such as amplitude, phase, frequency, and polarization modulators, as well as beam condenser and beam steering devices has hindered this frequency range from achieving its full exploitation. In this article, we aim to provide an overview of the basic principles and the main approaches which have recently been developed to overcome these hurdles with a specific focus on integrated devices capable of implementation in practical applications. Accordingly, works which involve external magnetic fields or cryogenic temperatures are not included. In order to overcome the typical poor material response in the THz, artificial resonances are commonly implemented in the device architecture in a large variety of approaches to boost the efficiency and increase the device miniaturization. Microelectromechanical systems (MEMS), plasmonic, or metamaterial subwavelength resonant features are the most commonly used methods which have proved to be successful in achieving this goal. Device tunability is obtained using a variety of approaches, for example, by introducing active materials, such as two-dimensional electron gas (2DEG), in standard semiconductor-based devices or bidimensional materials, whose optical properties, such as conductivity or transmittance, can be varied either optically or via electrical gating. In this review, the main avenues for achieving active amplitude, frequency, and polarization modulation in the THz frequency range are reported. This article is organized as follows. The first section is focused on the description of the basic theoretical concepts for engineering resonant features, such as metamaterial and plasmonic effects and their possible interplay with active tunable medium, such as graphene. In the second part, the focus is on the different device architectures and designs, for example, electronically or optically driven techniques. Amplitude, frequency, and polarization modulators are then reviewed, highlighting the principal figures of merit and the different modulator's performance. Finally, the implementation of this new class of optoelectronic devices in potential future applications in the scientific areas of spectroscopy, communication, and imaging is presented.

2 Basic theoretical principle

In a standard free electron gas model, the complex dielectric function $\varepsilon(\omega)$ can be described in terms of the frequency of the incident radiation ω, the plasma frequency ω_p, and the scattering time $\tau = 1/\gamma$ by the Drude model as follows:

$$\varepsilon(\omega) = 1 - \frac{\omega_p^2}{\omega^2 + i\gamma\omega} \tag{1}$$

The plasma frequency is given by $\omega_p^2 = Ne^2 / m_{eff}\,\varepsilon_0$, where N is the number density of electrons with charge e, ε_0 is the vacuum permittivity, and m_{eff} is the effective mass. For frequency $\omega < \omega_p$ (which lies in the ultraviolet spectral region for many common metals), the material has a negative ε and its behaviour is mainly described as "metallic". The AC conductivity $\sigma(\omega)$ is related to the DC value σ_0 through the equation $\sigma(\omega) = \sigma_0/(1 - i\omega\tau)$ [18]. To a first approximation this model can describe the behaviour of semiconductor materials under the illumination of photons with energies higher than the bandgap energy of the semiconductor. The density N of the photo-generated carriers is proportional to the fluence of the incoming radiation. Accordingly, for sufficient high fluences and frequencies lower than the scattering rate γ, the semiconductor can exhibit a "metallic" behaviour and a negative dielectric constant. Interestingly, even complex 2D materials such as graphene or MoS_2, whose bandgap depends on the number of layers [19, 20], can be described by the Drude model at THz frequencies in the first approximation. Graphene is a bidimensional material which derives much of its remarkable properties from its zero bandgap and conical energy dispersion. Extensive articles and reviews report on the electronic, optical, and plasmonic characteristics of these materials, which is now utilized in many research areas and applications. For the purposes of this review, it is interesting to focus on a few unique features of graphene, such as its high mobility and wide carrier concentration tuning range. Room temperature mobilities, which can be as high as ~10^5 $cm^2\,V^{-1}\,s^{-1}$ [21, 22], and carrier concentration modulations, up to ~10^{14} cm^{-2} [23], make graphene attractive because they provide a wider spanning range useful for active modulation. The optical conductivity in graphene at THz frequency is well described by the Kubo formula [24] considering only the intraband contribution. For more energetic photons, the interband contribution dominates reaching the well-known constant value of ~2.3% at higher frequency [25, 26]. The phenomenological scattering time parameter τ takes into account intraband phonon scattering, impurities, and defects in graphene. Its value varies in literature depending on the graphene quality, mobility, growth, and transfer methods, but it is normally between 0.2 and 1 ps [27–31]. Because the momentum relaxation time in graphene takes place over the sub-ps time scale, the optical

conductivity of graphene can be approximated by its electrical conductivity, which depends on the Fermi energy, which can be actively modified by optical pump/electrical gating. Therefore, the Drude model is often used as a good approximation for the optical conductivity in graphene.

The modification of the optical and plasmonic properties of the aforementioned materials allows for the engineering of devices, which can actively modulate the frequency, amplitude, and polarization of THz radiation. The first hurdle in designing an active THz modulation platform consists in the choice of the active material compatible with this frequency range. To overcome the lack of electromagnetic response in this frequency range and to increase the interaction with the materials, plasmonics and metamaterials have been widely used. Plasmonic resonant devices have been implemented across the whole frequency range, but they are particularly important in the THz range. Surface plasmon resonances are based on a solution of the Maxwell equation, which is fulfilled at the boundary between a material with a positive dielectric function and one, normally a metal or a highly doped semiconductor, with a negative one. The supported transverse magnetic (TM) modes have perpendicular electric field component which peaks at the boundary and exponentially decreases in the substrates, yielding a strong subwavelength radiation confinement which is normally used to boost the light-matter interaction. Similarly, metamaterials have been demonstrated in a variety of contexts and are the object of several reviews [32–39]. Whether they are excited through their magnetic or electrical response, these subwavelength objects exhibit an artificial resonance, which depends primarily from their shape and size rather than by the material choice. The modification of their geometry, or of their material properties through an active electronic input, optical modification, or mechanical deformation, defines the active principle of the various modulation approaches.

3 Modulator architectures

3.1 All-optical devices

One route to achieve an active modulation in the THz is the optical-induced modification of the device properties. The photo-generated carriers upon illumination of a pump beam produce a modification of the mobility and/or conductivity in the material, which is then probed by the THz radiation. Normally, photons carrying energy higher than the material bandgap are employed, which can be emitted by pulsed or continuous wave (cw) sources. The material of choice is typically silicon [40–43] or GaAs, which suggests the implementation of optical or near-infrared lasers, typically 800 nm centered broadband fs-pulsed lasers. In all these experimental situations, the main limits in modulation depth and speed are arising from the substrate material rather than the illumination sources. In fact, it is the carrier mobility, conductivity, and recombination times of the illuminated materials that dictate the limit, rather than the laser pulse duration. The recombination time of photo-generated carriers in silicon, which is reported to be >1 ms, ultimately limits the achievable modulation speeds. Different substrates, such as GaAs, and low temperature-grown GaAs have <1 ps recombination times, thus allowing faster modulation speeds. Resonant metamaterial [44] or arbitrary shaped designs [40] can be realized by opportunely masking or illuminating the semiconductor substrate. In Ref. [40], the potential of all-optical control has been demonstrated by implementing a spatial light modulator which modifies with a software the infrared light impinging onto a silicon wafer, thus achieving a photo-generated spatial distribution of carriers. The versatility of this method has been tested in a modified infrared pump/THz probe scheme to create an optical vortex or to test the spatial resolution of the device. Photo-pumping has been achieved with both cw and pulsed lasers emitting in the visible and near-infrared spectral regions. Several authors have reported different power, intensity, and fluence units and values depending on the experimental approach and the availability of instruments. The broadband modulation depth achievable without the insertion of any extra optical components such as the spatial light modulator can be as high as 98.6% for pump intensity >540 μJ/cm^2 [40] and ~100% for time-averaged pump powers >400 mW [41] with ~800 nm centered fs-pulsed lasers. By using 0.8 W pump power from a 1550 nm cw laser, the authors in Ref. [45] managed to achieve a modulation depth of 94% for graphene on germanium, significantly higher than the 64% reported for germanium alone. By implementing narrow-bandwidth, frequency-selective InSb gratings instead, a modulation depth of 46.7% for TM polarization at 1.5 THz has been reported in Ref. [46] for 120 mW pump power by using a 405 nm cw laser. The modulation depth under optical pumping for both cw and pulsed THz radiation was reported to improve after spinning a polymer on the silicon substrate [43]. The effect was attributed to the increased electron-hole, electron-phonon, and electron-impurities scattering at the organic/inorganic boundary. In Ref. [41], the authors demonstrated how the transfer of monolayer graphene on a silicon substrate was

beneficial in increasing the modulation depth achievable at lower pump powers. In fact, despite the well-known absorption of graphene in the visible and infrared spectral regions of approximately 2.3%, the authors reported in the broadband range 0.2–2 THz a modulation depth as high as 69% for a graphene on silicon substrate, significantly higher than the 45% achieved with the silicon wafer alone with the same pump power level of 40 mW, as shown in Figure 1. This effect was ascribed to the transfer of photo-generated carriers from the silicon substrate to the graphene layer, where they experience a much higher mobility, thus boosting the conductivity/absorption of graphene. A similar approach has also been reported with another bidimensional material, MoS_2, on silicon in Ref. [20]. The effect of annealed MoS_2 on silicon yielded, at a pump power of 1 W from a 808 nm cw laser, an improved modulation depth as high as 64.9% at 0.9 THz, three times higher than bare silicon. This effect was attributed to the trapping of photo-generated holes in MoS_2, which led to an increase of electron concentrations and conductivity in silicon. Germanium has also been proposed as a possible host material for the graphene transfer [45] in all-optical THz modulators reporting the remarkable performance of a maximum ~94% modulation depth and ~200 kHz modulation speed over a broadband 0.25–1 THz region. In contrast to the case of silicon, the increase in the modulation depth achieved by transferring graphene on top of germanium was attributed to nonlinear effects in the optical conductivity of graphene. Interestingly, because of the smaller band gap of germanium (0.66 eV) and higher carrier mobilities compared to silicon, it is possible to achieve considerable modulation depths at lower power levels and, mostly, with a 1.55 μm-wavelength laser, thus providing a direct link with the optical communication technology. InSb gratings on a semi-insulating (SI)-GaAs substrate have also demonstrated a THz response which could be tuned by a cw optical pump [46]. In this experiment, the pump irradiation allows the dynamic modification of the plasma frequency of the localized surface plasmon sustained by the gratings, rather than just an all-optical induced change in conductivity. Unlike the previous approaches, which were targeting a broadband response, plasmonic/metamaterial resonant metallic features are commonly used to boost the interaction with the substrate concentrating the light over subwavelength volumes in a smaller selective frequency range. One of the first successful demonstrations of a metamaterial split ring resonator (SRR) array fabricated onto a high-resistivity GaAs substrate as an efficient THz modulator was achieved through optically pumping at 800 nm with fs pulses [47]. The SRRs were arranged into arrays in order to facilitate efficient coupling of the THz radiation, while the photo-injected carriers were actively shorting the electrical resonance supported by this device. A modulation depth of ~60% was achieved, and the modulation speed was principally limited by the ~ps recombination time of the photo-generated carriers. In a further experiment, the same group demonstrated an optically pumped frequency-tuneable metamaterial design [48] showing a frequency tuning between 1.06 and 0.85 THz, albeit with an amplitude modulation. The main excited resonance was identified as the LC resonance, in analogy with electronic circuits, where the inductance L lies in the arms of the SRR, and the maximum E-field

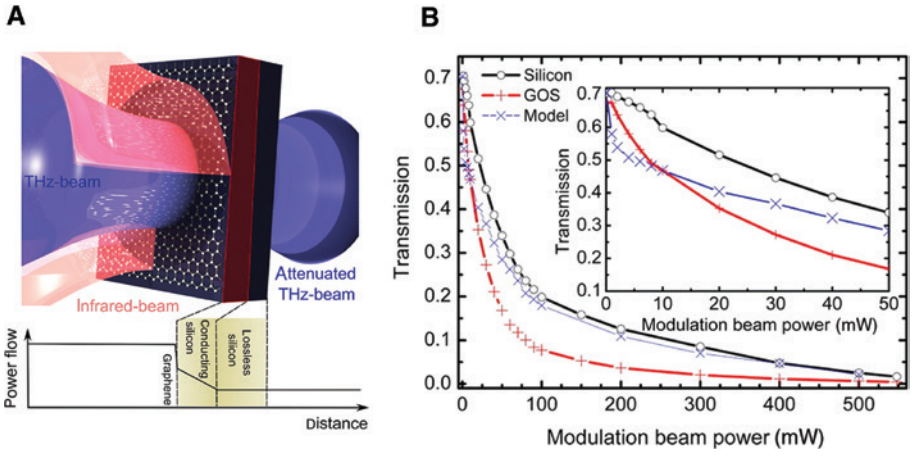

Figure 1: (A) Experimental sketch of the experiment. The pump beam induced photo-generated carriers in the silicon-graphene region, thus modifying the transmission for the THz beam. The effect of graphene transfer on silicon is evident in (B), where graphene on silicon (GOS) shows a stronger absorption and therefore allowed higher modulation depths at lower pump power levels. (Adapted with permission from P. Weis et al. ACS Nano 6, 9118-9124, 2012, Ref. [41]. Copyright 2012 American Chemical Society.)

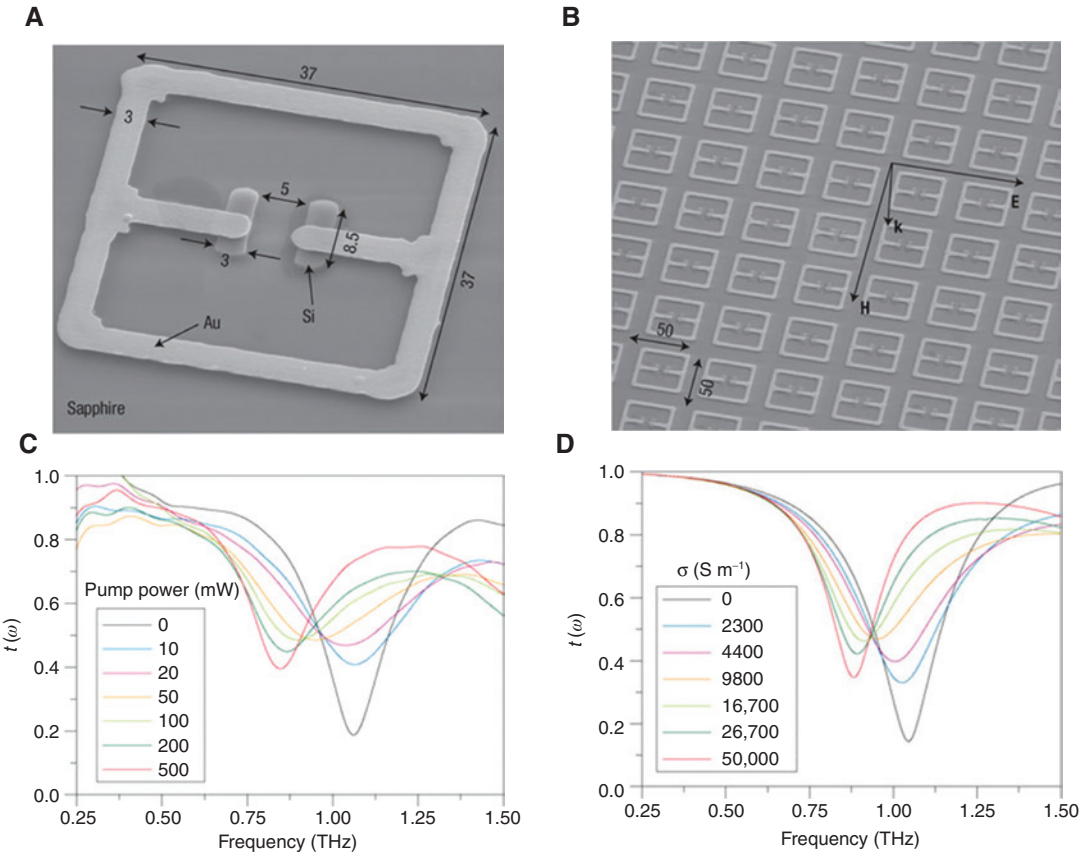

Figure 2: (A and B) SEM images of the single metallic/silicon SRR and an array. (C) The experimental frequency tuning achieved at different pumping levels and (D) the corresponding simulations. Figure adapted with permission from Macmillan Publishers Ltd.: Nature Photonics [48]. Copyright 2008.

is concentrated in the capacitor C gap. The resonant frequency ω_0 is in fact $\sim(LC)^{-0.5}$, and therefore, by changing the capacitance, it is possible to significantly act on the resonant frequency. The task was achieved by fabricating metallic split rings using silicon as the capacitor on top of sapphire substrate, as shown in Figure 2A and B. The optical excitation of photocarriers damped the resonance for low power levels, similar to Ref. [47]. However, for high pump power levels, the induced conductivity change was sufficient to turn the silicon capacitor plates into a "metallic" behaviour, which resulted in an effective change in the capacitor geometry and resonant frequency, as shown in Figure 2C and D.

3.2 All-electronic devices

In many applications, an all-electronic control is highly desirable. In fact, it eliminates the need of an extra laser source and relative driving electronics, allowing for a more compact design. Ref. [49] reported one of the first demonstrations of an all-electronic amplitude modulator operating at room temperature. The authors electronically depleted the carrier concentration of a 2DEG in a GaAs/AlGaAs interface by electrostatic gating. Although the reported modulation depth was limited to a few percent, this article reported the basic principle, which has been exploited further in combination with metamaterial resonant devices, constituting one of the major breakthroughs in the field [50, 51]. The integration of connected resonant metallic metamaterials forming a Schottky barrier with a 1-μm-thick n-GaAs layer over a SI-GaAs substrate [50] allowed the dynamical damping of the resonance. By electrostatically modifying the carrier concentrations, the resistance in the split gap was changed and a 50% modulation depth was achieved in transmission.

Other significant works which ignited the field by introducing graphene as an active medium are by Sensale-Rodriguez et al. [52, 53]. The low insertion losses and fast carrier recombination make this material extremely interesting for optical modulation, but its limited absorption, mostly in the visible spectral region, is clearly a hurdle to

the realization of large optical modulation depths. In the THz frequency range, absorption is mainly described by the intraband optical conductivity, which can be efficiently tuned by acting on the Fermi energy. On the basis of this principle, in Ref. [52] the authors demonstrated a simple, all-electrical-driven broadband THz modulator operating in transmission, based on graphene on SiO_2/Si substrate reporting a modulation depth of 15% and a modulation speed of ~20 kHz, limited by the parasitic RC constant of the device, which paves the way to real-world applications. In Ref. [53], the same authors further enhanced the modulation depth to 64% by changing the device architecture, schematically reported in Figure 3, to a reflection scheme and placing the graphene in the antinode of a standing wave. When the substrate optical thickness resulted in an odd-multiple of the THz radiation wavelength, a change in graphene conductivity resulted in large amplitude swings. Even though the modulation speed recorded was on the order of 4 kHz, this was limited by the device size and architecture rather than by any intrinsic physical properties of the material, such as the carrier recombination time. Recently, liquid crystal-based devices have attracted considerable attention as potential candidates for an integrated THz platform. The combination of nematic liquid crystals, such as isothiocyanate-based mixtures, which present low losses in the THz, with arrays of metallic metamaterials has been used for the realization of perfect absorbers [54], active amplitude/frequency modulators [55, 56], and has been proposed also for polarization modulators [57]. The ability of liquid crystals to orientate their dimers under an applied electric field, thus providing a dynamically tuneable birefringence as high as ~0.3, is at the basis of the active modulation. Amplitude modulators have been reported with modulation depths as high as 75% [55] and ~90% [56] and a peak frequency shift of ~7%. These devices operate in reflection, as the resonant metamaterial unit is structured as a metal-insulator-metal to allow for biasing of the liquid crystal layer. The compactness, versatility, and high modulation depths yielded represent the main advantages of this approach, while their speed, a more complex fabrication requirement, as they are intrinsically 3D objects, might be detrimental to their implementation in an integrated platform. Finally, even though the bias voltages required to drive liquid crystals-based THz modulators are on the order of a few volts, they are not likely to be reduced further because of the height of the unit cell and because of the Freedericksz transition threshold voltage.

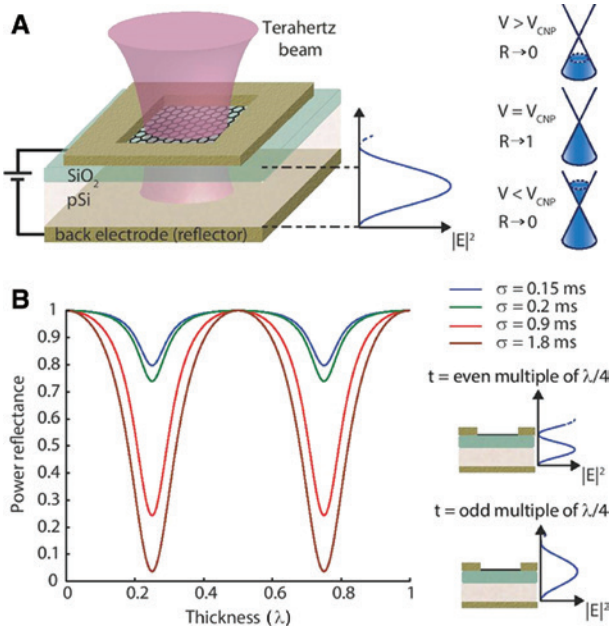

Figure 3: (A) Extraordinary modulation of the reflected terahertz radiation is achieved by modulating the Fermi energy of graphene electrostatically along the Dirac cone. (B) When the substrate thickness is an odd-multiple of the THz wavelength, this effect is maximized with the light at the antinode of a standing wave. (Reprinted and adapted with permission from B. Sensale Rodriguez et al. Nano Letters 12, 4518–4522, 2012, Ref. [53]. Copyright 2012 American Chemical Society).

3.3 Microelectromechanical systems

Metamaterials have played a large part in the development of THz devices due to their artificial resonances, which can be engineered by lithographic tuning of the metal geometry. As these resonances are fundamentally based on the structural dimensions of the metamaterial pattern, physically changing the shape of the resonant components in these arrays has a strong effect on the resonance conditions. MEMS have been used to physically alter the resonant components of individual unit cells in metamaterials, leading to the realization of active, electronically tunable THz devices [58–62]. MEMS are advantageous, as unit cells can be individually addressed electronically, increasing the range of tuning parameters. Also, because of the strong dependence of the metamaterial resonant frequency to the physical geometry, altering the resonator shape can have powerful modulation effects. These devices are typically built by depositing metal in a metamaterial array with some areas deposited onto a sacrificial layer which, when etched away, releases part of the metal from the substrate. This results in anchored microcantilevers, which typically curve away from the substrate. When a bias is applied, an electrostatic attractive force causes them to straighten towards the substrate due to the

high surface area-to-volume ratio, allowing for the electrical tuning of the metamaterial shape.

This tuning method is used by Pitchappa et al. [58] to independently tune the dark mode and the bright mode of a metamaterial resonator for electromagnetically induced transparency (EIT). This device employs a cut wire resonator (CWR), supporting a bright mode with a broad resonance at around 0.55 THz, and two SRRs (dark mode) with a sharper resonance at 0.55 THz, which can be excited by the CWR. As shown in Figure 4A, both of these components can be independently addressed and mechanically tuned by the application of a voltage. When both of these resonators are flat on the surface, EIT is observed with the destructive interference between the CWR and SRR resonances, resulting in a transmission peak at 0.55 THz. As the angle between the resonators and the substrate is increased, the resonance frequency of this transparency can be actively tuned, as reported in Figure 4B. By increasing the angle of the SRRs from the substrate while keeping the CWR on the substrate, a blue shift in the transmission peak is observed from 0.55 to 0.65 THz. Similar THz device designs are demonstrated in Refs. [59, 60] for the active control of the metamaterial frequency response. Both of these approaches employ a SRR metamaterial geometry with a movable capacitance arm on the application of a bias. The capacitance can be modified by tuning the angle that the capacitor arm makes with the substrate, resulting in large changes to the LC resonance frequency by over 50% as demonstrated in Ref. [59]. Alternatively, a vertically aligned capacitor is reported in Ref. [60] with an air gap which can be electrically tuned between two thicknesses with resonance frequencies at 0.45 and 0.7 THz, as shown in Figure 5A and B. The modulation mechanism is very effective and reaches 16.5 dB modulation depth, as shown by the dots in Figure 5C. The efficient excitation of

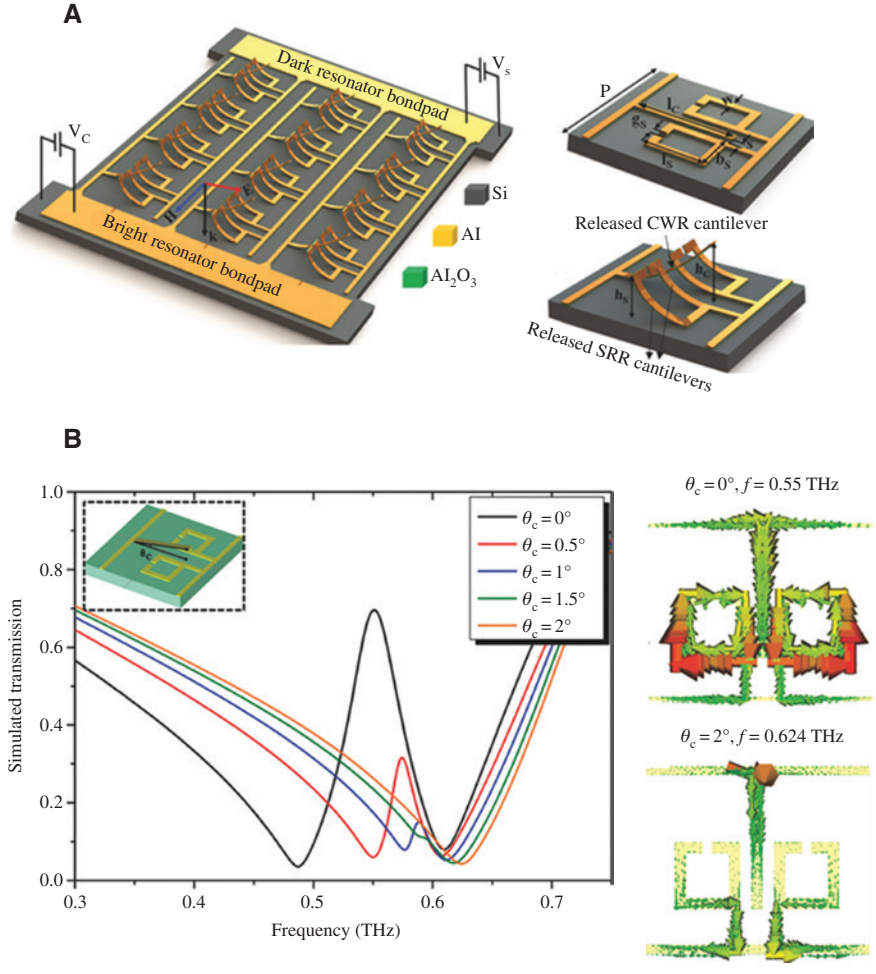

Figure 4: (A) Schematic of the EIT device based on the proposed MEMS metamaterial with independently reconfigurable microcantilevers, CWR, and metamaterial SRR, respectively. (B) Simulated transmission spectra of MEMS metamaterial, varying the angle θ_c of the CWR. The transmission window at 0.55 GHz for $\theta_c = 0$ degree disappears for $\theta_c = 2°$. The corresponding simulated surface currents in the two scenarios are also reported. Reprinted and adapted with permission from Pitchappa et al. [58].

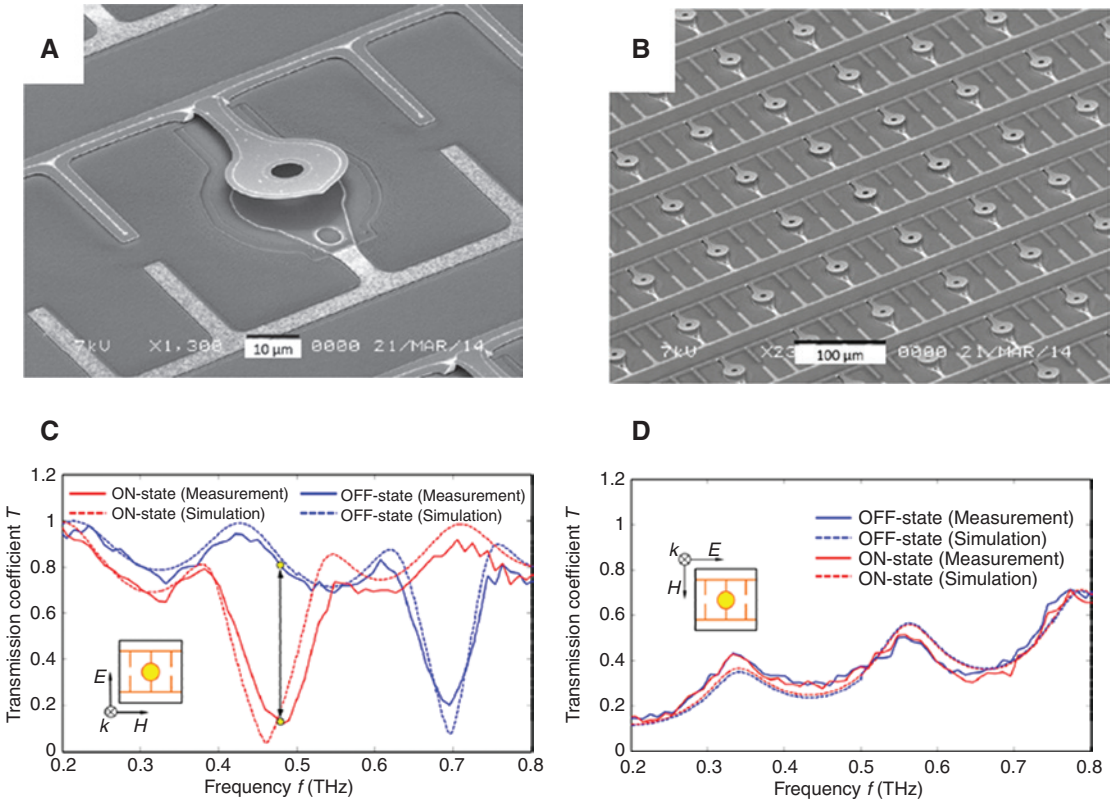

Figure 5: (A and B) MEMS SRR SEM images. (C) THz measured and simulated transmission characterization for incident E-field polarized along the cantilever in the off and on positions. (D) Similar characterization for E-field polarization perpendicular to the cantilever. Reprinted and adapted with permission from Han et al. [60], OSA.

the LC resonance of this device requires a component of the E-field polarization along the capacitor gap. An incident polarization perpendicular to the gap yielded, instead, a Drude-like flat response, as shown in Figure 5D. Another, non-electrical method of tuning the SRR capacitance is to deposit the metamaterial onto a deformable substrate. In Ref. [61], the authors deposited a metal resonator with a capacitive gap which can be tuned by stretching the sample. This resulted in repeatable frequency shifts of up to 6.6% at around 0.7 THz.

MEMS tuning is a very flexible way of building THz devices, as there are a myriad of possible design architectures to be employed. The LC resonance of SRRs is critically dependent on the capacitive gap, which has been taken advantage of to demonstrate large frequency shifts [59, 60]. There is, however, a fabrication limit to how small the geometry of such devices can be to operate efficiently, and most devices are observed to work under 1 THz as the surface area-to-volume ratio becomes unfavourable at higher frequencies. Modulation speed is an important parameter for many THz devices, especially for communication applications. Other approaches developed from RF MEMS, which are normally operating with ~μs time constants, are extending their operation frequency range up to 1 THz and probably, in the near future, beyond. However, we envisage that this approach cannot be efficiently extended further in frequency without affecting the other device performances, nor can it easily yield greater than megahertz (MHz) operation speeds. When dealing with physically moving parts, there is a limit to the modulation speeds which can be performed, with MEMS limited to modulation speeds between tens of kilohertz (kHz) and MHz, compared to the gigahertz (GHz) speeds required in typical communication environments.

4 THz modulators

4.1 Amplitude modulators

Amplitude modulators represent one of the principal building blocks in any integrated circuitry, and several approaches have been proposed to achieve this target. The main features which are desired can be tailored depending on the specific application, but a low driving voltage,

high modulation depth, fast reconfigurability, and ease of fabrication are common fundamental characteristics that every approach must address. In 2012, Lee et al. [63] demonstrated an integrated device operating at room temperature based on active graphene metamaterials. This compact device was fabricated by using meta atoms composed of metallic asymmetric double SRRs, monolayer graphene, polyimide dielectric spacers, and gating electrodes. By dynamically gating the graphene carrier concentration, the optical conductivity of the device was actively modified as demonstrated by the change in transmission recorded by a THz-TDS system. This work represented a breakthrough because for the first time a compact device was proposed which could be implemented on a printed circuit board with remarkable performances such as the 47% modulation depth and a 3 dB roll-off frequency of 12.6 MHz. However, the charge neutrality point of graphene was found at ~350 V, and comparable voltages were required in order to drive this modulator, thus strongly restricting any possible implementation of such a device. This issue has been addressed by two groups [56, 57] aiming to achieve a low-bias driving voltage. In 2013, Valmorra et al. [64] reported a THz modulator with a simple fabrication process based on metallic metamaterial SRRs arranged in arrays on top of graphene, which was grown by chemical vapour deposition and transferred on top of a SiO_2/Si substrate. By electrostatically changing the graphene conductivity along the charge neutrality point, they demonstrated ~12% modulation depth at ~10 V bias. The authors in Ref. [65] implemented a double-gate architecture where the SRRs were not only providing the THz resonant response, but also the local top-gate was being electrically separated from graphene by a ~30 nm SiO_2 dielectric layer. The modulation depth of ~18% was similar to that of the previous work of Ref. [64], but it was achieved with the ultra-low voltage bias value of ~0.5 V. The modulation speed of this type of device has also been a matter of investigation by several groups. Broadband sources, such as THz-TDS systems or fast Fourier transform spectrometers, are limited to operating frequencies of typically ~1–100 kHz and therefore are not the most suitable sources for the determination of the cutoff frequency for modulation speeds in the MHz region. Conversely, THz QCLs offer a stable, powerful narrow frequency source, which is ideal for this task. In Ref. [66], the authors managed to integrate a graphene-based modulator on top of a QCL, which could independently modulate the emitted THz radiation with a 3-dB cutoff frequency >100 MHz and with a ~100% modulation depth. The basic device architecture is reported in Figure 6A and the modulation speed characterization in Figure 6B. This is of fundamental importance for reducing the chirping and frequency instabilities caused by a direct modulation of the laser bias, which would hinder the use in practical applications. The miniaturization of the device was key in order to reduce all the capacitances and impedances in the circuit, which otherwise would limit the modulation speed. Interestingly, in this work, an indirect measurement of the frequency roll-off was

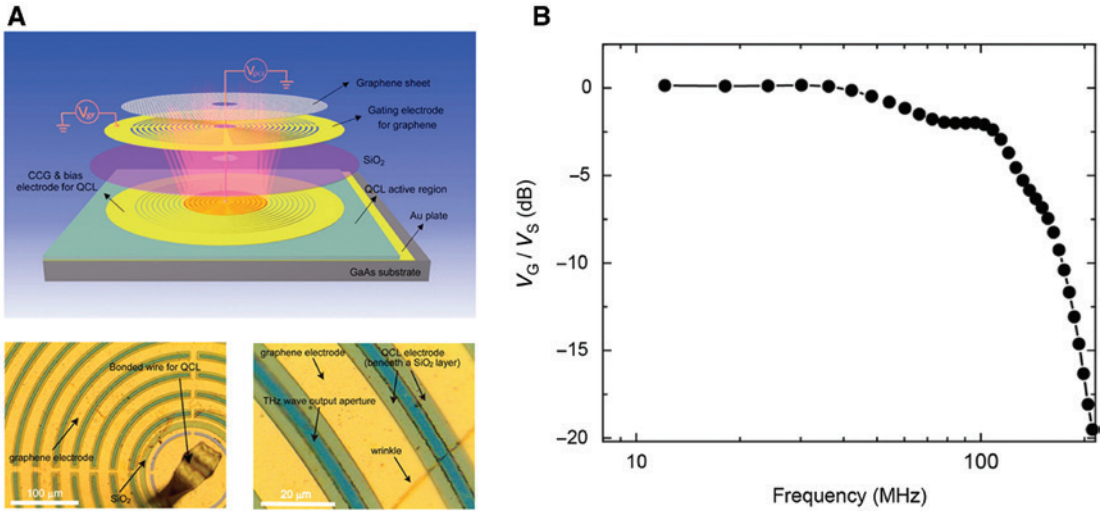

Figure 6: (A) Schematic of the graphene modulator integrated with quantum cascade lasers and optical pictures of the real device. The inner central rings are connected to the top surface of the QCL for biasing the device, while the outer ones contacting the graphene are used for modulating the emission. (B) Frequency response of the graphene modulator, where V_S and V_G are the amplitude of the voltage on the graphene electrode and that applied to the graphene sheet, respectively. Reprinted and adapted with permission from Liang et al. [66].

proposed, which was developed in parallel by the group in Cambridge [67, 68], working on the realization of graphene/plasmonic amplitude modulators operating external to the cryostat based on antenna and interdigitated bow-tie arrays. The advantages of an external modulation scheme lie in the possibility of modulating different frequencies separately, paving the way for independent frequency and phase modulation in quadrature with a single source. This approach yielded a lower modulation depth, ~20–30%, but a similar performance in modulation speed >110 MHz with a QCL emitting at 2 THz [68]. The design of any efficient optical modulator based on plasmonic/metamaterial requires a precise knowledge of the graphene electrical conductivity range, which can be tuned. This is required to maximize the interaction with the plasmonic/metamaterial features and to avoid an excessive damping of the resonance. Furthermore, the realization of high-speed modulation is strongly related to the size of the modulator and to the radiation frequency. A device size reduction of the modulator is clearly beneficial but is ultimately limited by the need to achieve efficient radiation coupling and by diffraction. A detailed circuit analysis is also required in order to identify all the possible limitations to the cutoff frequency, such as parasitic capacitances and substrate resistivity. In Ref. [67], the large capacitance of the graphene areas limited the modulation speed to ~5.5 MHz. In the architecture reported in Ref. [68], the graphene regions were reduced to arrays of a few μm^2 areas shunting the bow-tie arms, thus achieving the >110 MHz modulation speed, which was still limited by the parasitic capacitance introduced by the metallic contact pads. A schematic of the device is reported together with scanning electron microscope (SEM) images of the graphene/bow ties in Figure 7; the graphene regions are clearly distinguishable in the inset.

Electronically tuneable 2DEG-based devices represent a parallel and viable route to achieving integrated amplitude modulators which yield excellent performances in high-speed modulation and modulation depths. Recent works targeted mostly the sub-THz frequency range [69, 70], aiming at a direct monolithic integration of the modulators onto a chip with a view to a THz circuitry platform for communications. In Ref. [69], the authors propose a 2DEG supported in an InGaAs layer separated from a THz slot waveguide by an AlGaAs spacer as a reconfigurable lossy channel. The high degree of interaction offered by the impedance matched slot waveguide, between the THz radiation and the channel whose conductivity can be efficiently modified with <2 V bias, yielded remarkable performances. At 0.25 THz, ~96% modulation depth was reported with a ~14 GHz cutoff frequency. A schematic of the device material and architecture together with a top-view picture of the real device are reported in Figure 8. In Ref. [70], the authors demonstrated more than 1-GHz modulation speed (even though significant degradation was observed already above 200 MHz) and 86% modulation depth. In this work, InAlN/AlN/GaN/AlN/GaN double-channel heterostructures supported a 2DEG channel

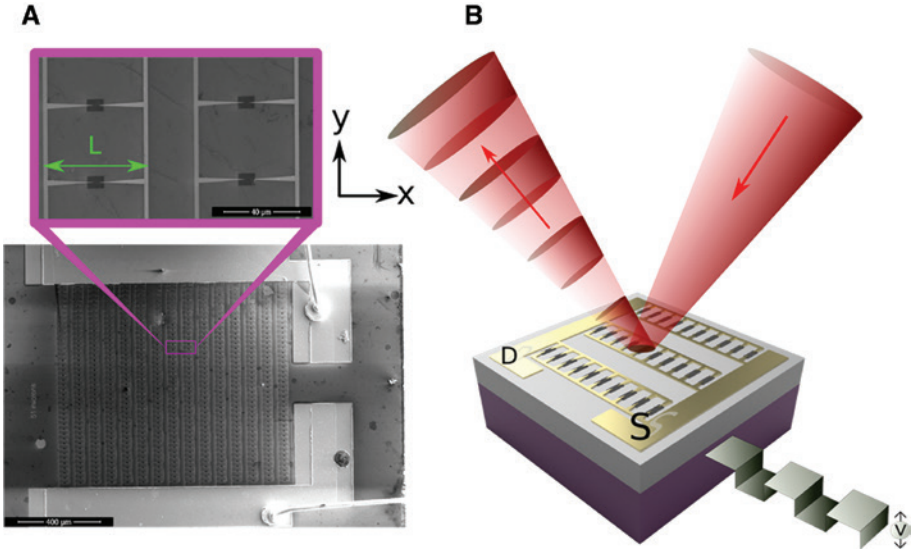

Figure 7: (A) SEM image of the device. The interdigitated scheme is based on metallic bow tie fabricated with two metals with different work functions, namely, Pd and Ti, shorted by rectangular regions of graphene, as clearly seen in the inset. (B) Basic operating principle of the device. The device can be operated both as a modulator [68] and as a detector [13]. Reprinted from Jessop et al. [68], with the permission of AIP Publishing.

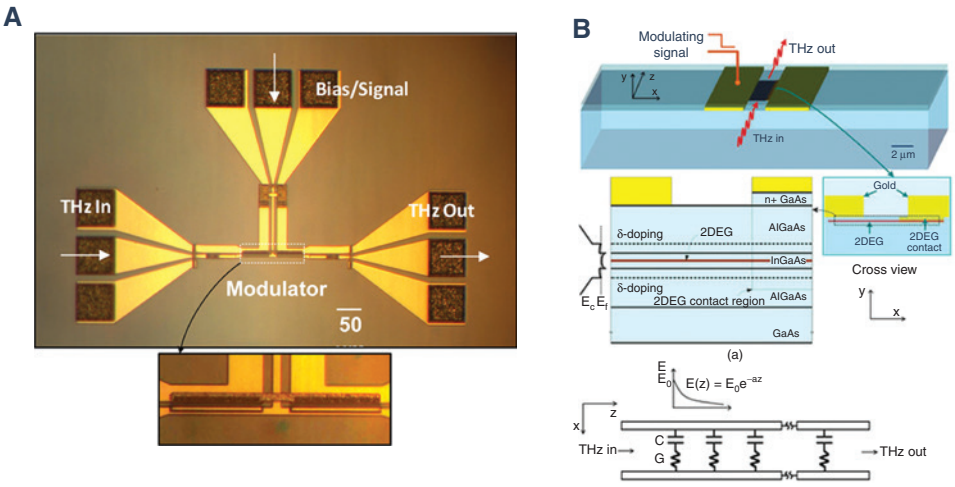

Figure 8: (A) Optical micrograph image of the real device. (B) Schematic of the THz modulator device based on slot waveguide and 2DEG; material composition and equivalent electronic circuit are reported as well. Reprinted and adapted from Singh and Sonkusale [69].

whose interaction with a metallic grid based on dipolar resonances is the modulation scheme. A single unit consisted of a capacitor integrated with the 2DEG via the ohmic contacts, while a Schottky gate is used to change the conductivity in the channel. By turning the 2DEG channel on and off, the frequency response of the device oscillates between two different frequencies. A similar approach has recently been reported by integrating monolayer graphene in the center of a dielectric SiO_2/Si-based slot waveguide reporting a 90% modulation depth below 1 THz with a 2 kHz cutoff frequency [71]. A brief summary of the different works on amplitude modulators is shown in Table 1.

4.2 Frequency modulators

There are a few mechanisms which can be implemented in order to achieve an integrated frequency tuning. Several strategies have been adopted which either modify the resonant circuit fundamental components [48] or induce a change in the plasmonic resonances in the semiconductor [46] and 2D materials [73–76] or directly alter the structure of the resonant elements [59]. Graphene is well known to support surface plasmons [73] in the THz, and it has been proposed as a building block for the realization of an integrated platform at these frequencies [77]. However, even though the resonant modes supported by gratings [75] and anti-dot arrangements [76] have a tunable frequency dispersion, they typically yield limited modulation depths (<10%), making these approaches not viable for the building of an efficient modulation platform. Other elegant methods rely on the optical interplay between dark and bright modes in more complex metamaterial architectures, reminiscent of the electromagnetically induced transparency [58, 78].

In Ref. [78], the authors managed to induce a transparency window and achieve an active control over the group delay and group refractive index of THz pulses. However, in several applications, for example, spectroscopy, a continuous tuning of the resonant frequency is required over ideally hundreds of GHz, and therefore, this interesting approach might be more suited for fundamental research. At the same time, efficient tuning with MEMS for frequencies higher than 1 THz is normally hindered by the difficulties connected with the fabrication of the resonant objects. An all-electronic or all-optical induced change in the dispersive properties of surface plasmon-based resonators is a more promising method to achieve a frequency modulation. Resonant surface plasmon features have a typical dispersion which scales $\propto n^{1/2}/w^{1/2}$, where n is the carrier concentration and w is the spatial periodicity. Graphene plasmons, instead, scale as $n^{1/4}/w^{1/2}$ [73–75]. In Ref. [75], the change in transmission, normalized to the transmission at the Dirac point, was however limited to a few percent. An interesting solution to overcome the limited coupling of light radiation and to increase the absorption and the modulation depth of bare graphene has been proposed by the authors in Refs. [79, 80]. In Ref. [79], the authors demonstrated how metallic slits with graphene concentrated in slot regions with subwavelength sizes strongly increased the absorption. The resonances are independent from the periodicity of the metallic grating but interestingly exhibit the same dispersion characteristics of pure

Table 1: THz amplitude modulator works, approaches, and basic performances.

Work	Description	Year	Frequency (THz)	Modulation depth	Modulation speed
Chen et al.	Metamaterial, 2DEG, all- electronic [50]	2006	0.72	50%	>1 kHz
Chen et al.	Metamaterial, 2DEG, all-electronic [51]	2009	0.81	80%	>2 MHz
Sensale-Rodriguez et al.	Graphene, all-electronic [52]	2012	Broadband	15.2%	20 kHz
Sensale-Rodriguez et al.	Graphene, all-electronic [53]	2012	0.62	64%	4 kHz
Jessop et al.	Graphene, bow-tie antennas [68]	2016	2	~20%	110 MHz
Liang et al.	Graphene integrated with QCLs [66]	2015	3.2	100%	110 MHz
Valmorra et al.	Metamaterial and graphene [64]	2013	Broadband	11.5%	–
Liu et al.	All-electronic, metamaterial, and graphene [72]	2015	4.7	60%	40 MHz
Singh and Sonkusale	Integrated chip and 2DEG [69]	2017	Broadband (<1 THz)	96%	14 GHz
Lee et al.	Integrated metamaterial and graphene [63]	2012	~0.8 THz	47%	~12 MHz
Wen et al.	All-optical (graphene on Ge) [45]	2014	Broadband (<1 THz)	94%	200 kHz
Weis et al.	All-optical (graphene on Si) [41]	2012	Broadband (<1 THz)	99%	–
Unlu et al.	MEMS [62]	2014	Broadband (>1.5 THz)	70%	20 kHz

graphene ribbons, as shown in Figure 9. This anomalous dispersion and increased absorption have been attributed to a larger optical matching of these resonant structures, where the metallic features act as a reservoir of electrons and the inductance is mainly concentrated in the gap region where the graphene is located. The modulation depth achieved is only ~15%, but the frequency tunability demonstrated is larger than 1 THz, even though not independent from the amplitude modulation. This approach is promising in light of its ease of fabrication and potential for higher modulation depths, which are supposed to reach larger values for high-mobility graphene. Increasing the modulation depth and dispersion with higher mobility values is justified by the inductive rather than resistive graphene behaviour in these architectures. Another novel and promising approach for frequency tuning has been recently proposed in Ref. [72]. The device architecture is based on complementary SRR (C-SRR) arrays strongly coupled to graphene ribbons, supporting surface plasmon resonances with frequencies close to the C-SRR resonances. The graphene ribbons are fabricated in the center of the C-SRRs in order to maximize the coupling between the two resonances. This hybrid system can be described by two Lorentz oscillators, and the coupling strength determining the frequency positions of the two peaks can be efficiently tuned by acting on the carrier concentration of the graphene. This approach not only offers a unique platform for the investigation of strong-light matter interaction but also yields remarkable performance in terms of modulation depth (~60%) and speed (~40 MHz) with a 4.7-THz QCL laser. A schematic design of the resonant hybrid C-SRR graphene arrays is shown in Figure 10 together with the modulation depth measured with a 4.7 THz QCL.

4.3 Polarization modulators

To influence the polarization of incident radiation in the THz regime, multilayer chiral metamaterials are commonly used because of the built-in handedness of these materials. Chirality, in geometric terms, defines a pattern which has no lines of mirror symmetry along its plane. Chiral metamaterials have an asymmetrical interaction with the left- and right-handed circular polarization components of incident radiation and can be lithographically tuned to exhibit circular dichroism, optical activity, non-reciprocal transmission, and/or negative refractive index [81]. These chiral designs can be tuned to rotate the polarization of incoming radiation or to convert from linear to circular polarizations.

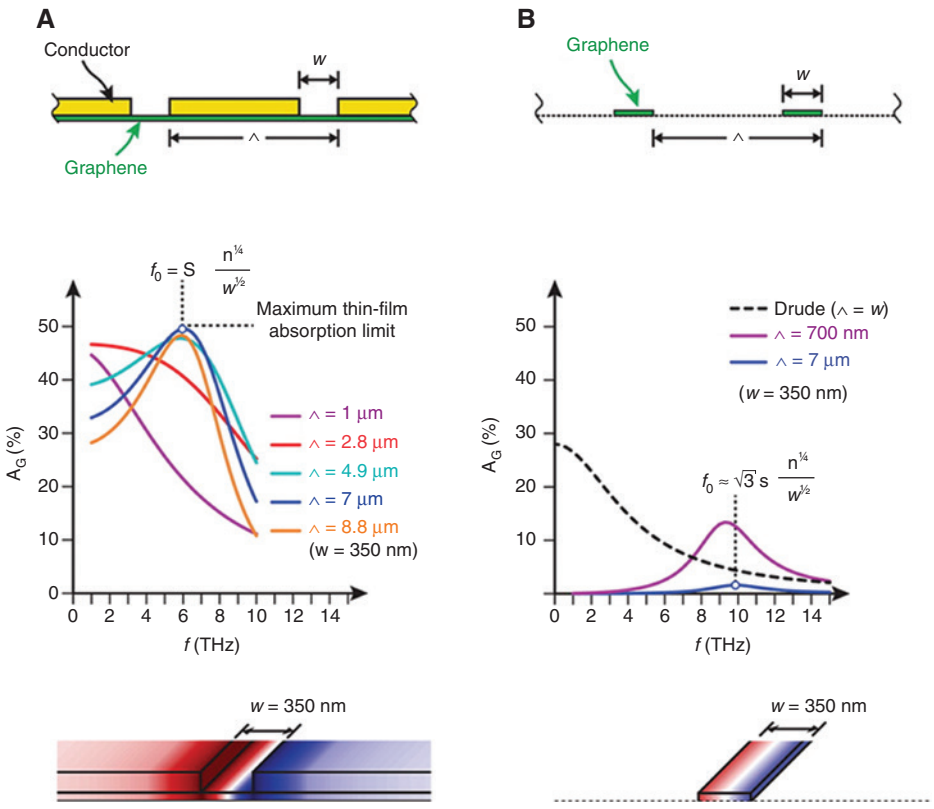

Figure 9: (A) Schematic of the hybrid structure composed of metallic conductor grating shorted by subwavelength graphene areas and the corresponding bare graphene ribbons (B). Both designs support surface plasmon resonances following similar trends by varying size and carrier concentration, but with different absorption and interaction with the incident radiation. (Reprinted and adapted with permission from Jadidi MM, Sushkov AB, Myers-Ward RL et al. Tunable terahertz hybrid Metal-Graphene Plasmons. Nano Lett. 2015, 15, 7099–7104, Ref. [79]. Copyright 2015 American Chemical Society).

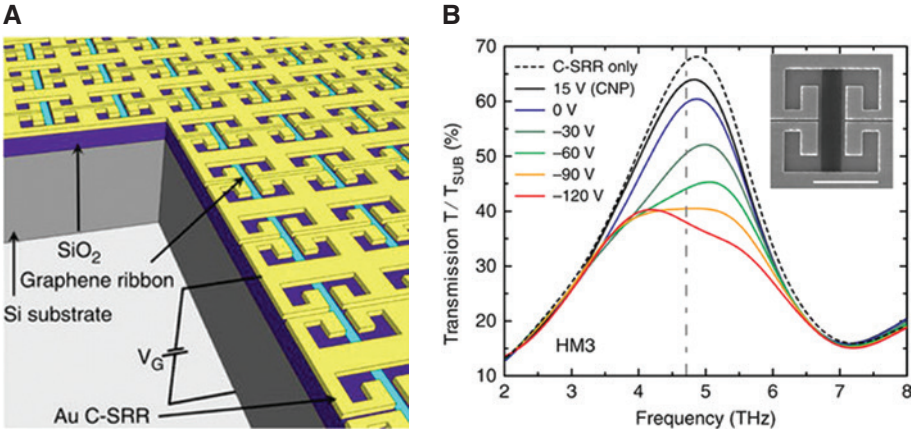

Figure 10: (A) Schematic design of the hybrid graphene C-SRR device. The graphene ribbons are positioned in the center of the C-SRR to maximize the coupling between the two resonances. (B) Modulation depth performance; it is possible to observe the anti-crossing between the two resonances for different biases of the graphene. Reprinted and adapted from Liu et al. [72].

For this purpose, these metamaterial structures are generally required to be 3D in nature, as their functional mechanism is based on inducing circulating currents with a normal vector along the plane of the device. The simplest way of building a metamaterial with an out-of-plane component is to use a bilayer design with a dielectric spacer layer between two metamaterial structures. Such a design was adopted by Zhou et al. [82] to build a device which can actively tune the polarization rotation of incident radiation. Figure 11A shows this

bilayer design, with the circulating currents inducing a magnetic moment anti-parallel to the incident electric field, resulting in a maximum linear polarization rotation of >12° for an incident laser fluence varying from 0 to 40 μJ/mm², respectively. The ellipticity of the transmitted radiation remains below 0.15 throughout. For the active control of this device, the bottom resonators sit on individual silicon islands which can have photocarriers excited by near-infrared femtosecond laser pulses. The conductivity of the silicon layer increases with the incident laser power, and the metamaterial response is dampened as result, reducing the polarization rotation effect. Larger dynamical polarization tuning of 23, 28, and 45 degrees can be achieved by acting on the interplay between the resonances of the two elements, as reported in Figure 11B, to the expense of an increased ellipticity. This value defines the polarization state of the radiation and is given by the ratio of the semi-minor and the semi-major axis of the elliptically polarized radiation, with values of 1 and 0 indicating the extreme cases of circular and linear polarized radiation.

Zhang et al. [83] describes a similar 3D device which uses metal pillars to construct the required out-of-plane component. The structure and the main performances of this device are shown in Figure 12. This device can switch its chirality handedness by the excitation of silicon optoelectronic switches within the metamaterial structure. In this design, the silicon, instead of being used to dampen the metamaterial resonance, was strategically placed to short circuit different parts of the metal structure when photo activated, modifying the metamaterial resonance condition. When linear polarization radiation is incident, this device will transmit elliptically polarized radiation. The handedness of this radiation and the direction of the semi-major axis are flipped upon photoexcitation of the silicon at two different frequencies, 1.0 and 1.1 THz. This device, therefore, demonstrates a fabrication technique which could be used to build a photo-active tunable circular polarizer in the THz regime. Kan et al. [84] uses a different tuning method which involves the enantiomeric switching of MEMS spirals to rotate the polarization of incident

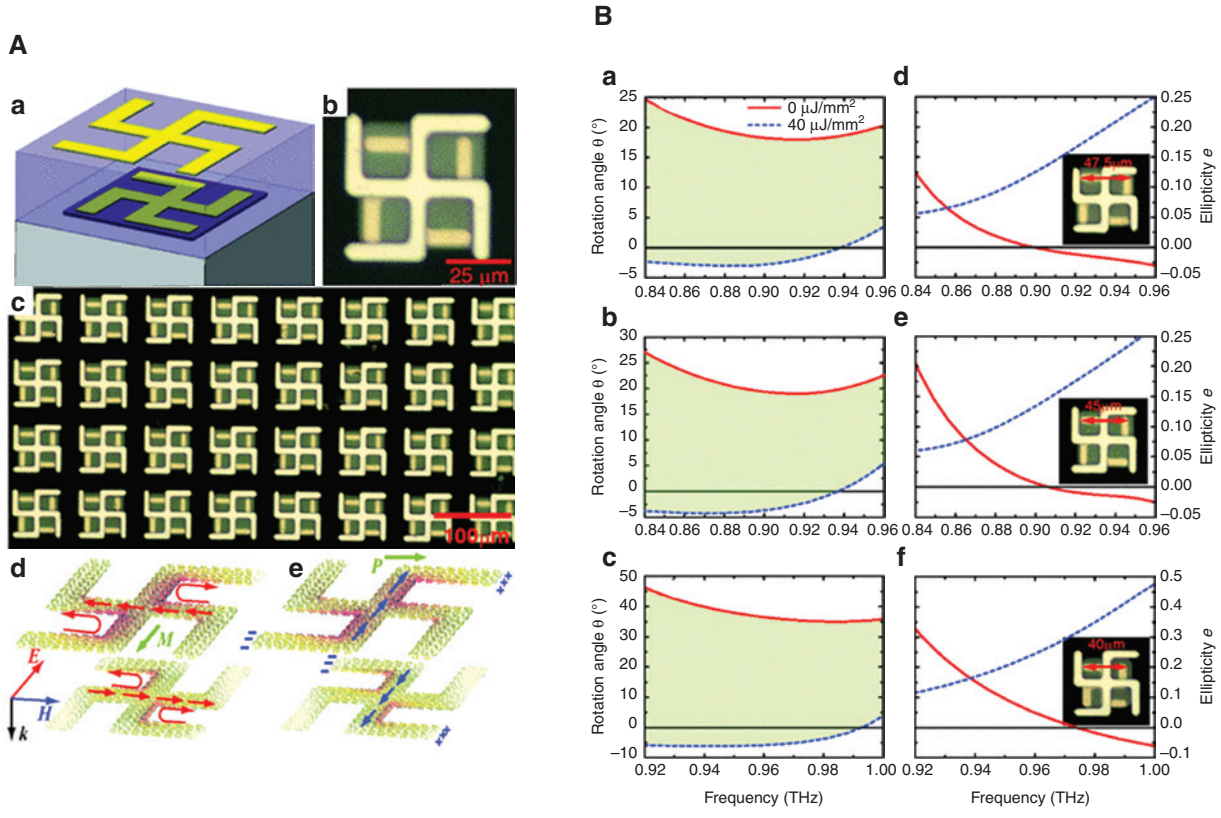

Figure 11: (A) Schematic of the unit cell based on the two controversial metallic designs separated by a dielectric spacer. The flow of the surface currents induced in the chiral metamaterial device and the induced magnetic (M) and electric (P) dipole momentum are also reported. (B) Dynamical characterization of the chiral device for different sizes of the bottom resonator. The rotation angles and ellipticities are reported when the laser was on (red line) and off (blue line). Reprinted figures with permission from Zhou J, Chowdhury DR, Zhao R. et al. Phys. Rev. B 86, 035448, 2012, Ref. [82], https://doi.org/10.1103/PhysRevB.86.035448. Copyright 2012 by the American Physical Society.

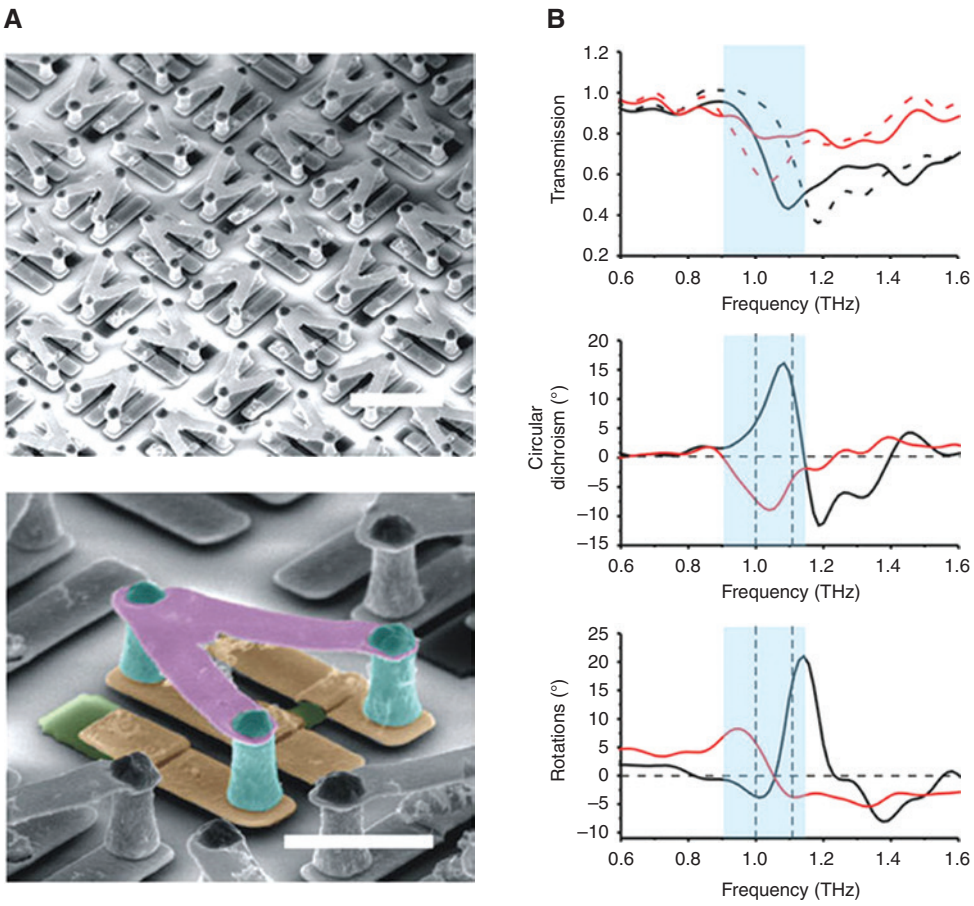

Figure 12: (A) SEM images of the fabricated chiral metamaterial. The scale bar is 25 and 10 μm for the top and bottom panels, respectively. The purple, blue, and yellow colours represent the gold structures at different layers, and the two silicon pads are shown in green. (B) The top panel shows the measured transmission spectra of left-handed (solid) and right-handed (dashed) circular polarizations, without (black) and with (red) photoexcitation.The middle panel shows the ellipticity, and the bottom panel the polarization rotation angle arising from the transmission-phase difference without (black) and with (red) photoexcitation. Figure reprinted and adapted with permission from Macmillan Publishers Ltd.: Nature Communications [83]. © 2008.

radiation. A deformable MEMS spiral can be pushed inwards or outwards by applying a pressure differential between both sides of the film. Spirals exhibit chirality because of the inherent handedness of the structure and can be tuned to exhibit optical activity, rotating the polarization of incident radiation. As the handedness of the spiral can be flipped by changing the pressure, the handedness of the chirality will also be switched resulting in bi-directional polarization angle tuning. The displacement of the spiral from the surface also determines the extent of the rotation angle applied, and hence, the output polarization can be smoothly tuned from an angle of +30 to –30 degrees for incident radiation at around 1 THz by varying the pressure differential. These chiral metamaterial systems are useful because of the flexibility of lithographic tuning and the scalability of the designs; however, making a broadband THz device for polarization modulation is not possible using this technique. The chiral properties of these structures, for example, the optical activity and circular dichroism, are only observed at specific wavelengths around the metamaterial resonance frequency. The device design is complicated further by the fact that strong control over the ellipticity and angle of the output polarization requires simultaneous control over both the phase and amplitude of the orthogonal polarization components, which is a highly non-trivial design task.

5 Applications

THz communications represent one of the main interest driving research in this area. Larger bandwidths, according to the Shannon theorem, are supposed to allow transmission with data rates exceeding 100 Gbit/s

[85], and the THz range is currently a non-allocated frequency. THz frequencies have been proposed for space communications, for example, between geostationary satellites [86, 87]. For ground communications, because of the limitation introduced by atmospheric absorption, different architectures can be put in place according to the transmission requirements, depending if long distances (attenuations <10 dB/km) or short ranges are required. Necessary considerations include the compatibility with all the other components of a THz circuitry, principally waveguides and detectors, which contribute in determining, alongside with cost, size, power consumption, and performances, the most suitable architectures. In the sub-THz frequency range, mostly in the 200–300 GHz range where powerful electronic sources exist and standard waveguides exhibit acceptable losses, an all-electronic integrated approach such as the one reported in Ref. [69] might be a more immediate route for the realization of amplitude modulators. It reports excellent performance in terms of modulation speed (~14 GHz) and depth (~96%), and it shows compatibility with existing technology. For frequencies above 2 THz, atmospheric absorption limits the transmission signals to local communications. THz communications can still be implemented for wireless hotspots in public places, such as hospitals or Universities, or for fast communications between mobile devices or for backhauls between the main network backbone and the local subnetworks. Above 2 THz, where for instance standard detectors and waveguides start to exhibit a poor efficiency, plasmonic/metamaterial devices integrated with 2DEG or graphene seem to be the more robust and valid approach.

Amplitude, frequency, and polarization modulators not only are the basic components in any future communication technology but also are in great demand for spectroscopic applications. The target is not only the molecular rotation transitions in gases but also the crystalline phonon vibrations and the intermolecular stretching and torsional modes. In THz solid-state spectroscopy, fast polarization rotators are of fundamental importance, for example, for the investigation of material chirality [88] and of novel materials (e.g. topological insulator properties) [89]. It is worth mentioning the importance of this new class of device for amplitude and frequency stabilization of QCLs in metrological grade spectroscopy [90–93]. Naming all the possible applications of THz active devices in gas- and solid-state spectroscopy, from sensing to healthcare to investigation of novel state of matter and materials, could be per se the topic of another review, as the one reported recently in Ref. [93].

6 Conclusion

In conclusion, we have presented an extensive review of all-integrated amplitude, frequency, and polarization modulators operating in the THz frequency range. In particular, the main methods which have been put through in order to achieve efficient modulators have been described, from all-optical to all-electronic and MEMS approaches. While the first two achieved similar figures of merit in terms of modulation speed and depth, MEMS are intrinsically slow and difficult to scale over the whole THz range, even though they are highly efficient. An all-electronic approach allows a higher degree of miniaturization, offering favourable performance in terms of equipment and power consumption over an all-optical approach. Finally, in this vibrant and fast-evolving field, amplitude modulators have already reached a high level of maturity, showing remarkable performance. The different final application requirements are now defining the modulator architectures. Conversely, frequency and polarization rotators, which would have a large impact in several research fields, are intrinsically more complex to be engineered and have not yet been exploited to their full potential.

Acknowledgments: The authors acknowledge financial support from the Engineering and Physical Sciences Research Council (Grant no. EP/J017671/1, Coherent Terahertz Systems).

References

[1] Sirtori C. Applied physics: bridge for the terahertz gap. Nature 2002;417:132–3.
[2] Tonouchi M. Cutting-edge terahertz technology. Nat Photonics 2007;1:97–105.
[3] Nagatsuma T, Ducournau G, Renaud CC. Advances in terahertz communications accelerated by photonics. Nat Photonics 2016;10:371–9.
[4] Wun JM, Lai CH, Chen NW, Bowers JE, Shi JW. Flip-chip bonding packaged THz photodiode with broadband high-power performance. IEEE Photon Technol Lett 2014;26:2462–4.
[5] Köhler R, Tredicucci A, Beltram F, et al. Terahertz semiconductor-heterostructure laser. Nature 2002;417:156–9.
[6] Rösch M, Scalari G, Beck M, Faist J. Octave-spanning semiconductor laser. Nat Photonics 2015;9:42–7.
[7] Jung S, Hyun Kim JAE, Jiang Y, Vijayraghavan K, Belkin MA. Terahertz difference-frequency quantum cascade laser sources on silicon. Optica 2017;4:38–43.
[8] Lu Q, Wu D, Sengupta S, Slivken S, Razeghi M. Room temperature continuous wave, monolithic tuneable THz sources based on highly efficient mid-infrared quantum cascade lasers. Sci Rep 2016;6:23595.

[9] Jung S, Jiang A, Jiang Y, Vijayraghavan K, Belkin MA. Broadly tunable monolithic room-temperature terahertz quantum cascade laser sources. Nat Commun 2014;5:4267.
[10] Nagatsuma T, Horiguchi S, Minamikata Y, et al. Terahertz wireless communications based on photonics technologies. Opt Express 2013;21:477–87.
[11] Koppens FHL, Mueller T, Avouris P, Ferrari AC, Vitiello MS, Polini M. Photodetectors based on graphene, other two-dimensional materials and hybrid systems. Nat Nanotech 2014;9:780–93.
[12] Sun Z, Chang H. Graphene and graphene-like two-dimensional materials in photodetection: mechanisms and methodology. ACS Nano 2014;8:4133–56.
[13] Degl'Innocenti R, Xiao L, Jessop DS, et al. Fast room temperature detection of terahertz quantum cascade lasers with graphene loaded bow-tie plasmonic antenna arrays. ACS Photon 2016;3:1747–53.
[14] Cai X, Sushkov AB, Suess RJ, et al. Sensitive room-temperature terahertz detection via the photothermoelectric effect in graphene. Nat Nanotech 2014;9:814–9.
[15] Degl'Innocenti R, Xiao L, Kindness SJ, et al. Bolometric detection of terahertz quantum cascade laser radiation with graphene-plasmonic antenna arrays. J Phys D: Appl Phys 2017;50:174001.
[16] Yariv A. Quantum electronics. 3rd ed. New York, USA, John Wiley and Sons, 1989, pp. 307–313.
[17] Degl'Innocenti R, Majkic A, Vorburger P, Poberaj G, Günter P, Döbeli M. Ultraviolet electro-optic amplitude modulation in β-BaB_2O_4 waveguides. Appl Phys Lett 2007;91:051105.
[18] Maier SA. Plasmonics: fundamentals and applications. New York, USA, Springer, 2007, p. 15.
[19] Chen S, Fan F, Miao Y, He X, Zhang K, Changa S. Ultrasensitive terahertz modulation by silicon-grown MoS_2 nanosheets. Nanoscale 2016;8:4713–19.
[20] Cao Y, Gan S, Geng Z, et al. Optically tuned terahertz modulator based on annealed multilayer MoS_2. Sci Rep 2016;6:22899.
[21] Boyd DA, Lin WH, Hsu CC, et al. Single-step deposition of high-mobility graphene at reduced temperatures. Nat Commun 2015;6:6620.
[22] Banszerus L, Schmitz M, Engels S, et al. Ultrahigh-mobility graphene devices from chemical vapor deposition on reusable copper. Sci Adv 2015;1:e1500222.
[23] Efotov DK, Kim P. Controlling electron-phonon interactions in graphene at ultrahigh carrier densities. Phys Rev Lett 2010;105:256806.
[24] Gusynin VP, Sharapov SG, Carbotte JP. On the universal ac optical background in graphene. New J Phys 2009;11:095013.
[25] Dawlaty JM, Shivaraman S, Strait J, et al. Measurement of the optical absorption spectra of epitaxial graphene from terahertz to visible. Appl Phys Lett 2008;93:131905.
[26] Freitag M, Low T, Xia F, Avouris P. Photoconductivity of biased graphene. Nat Photonics 2013;7:53–9.
[27] George PA, Strait J, Dawlaty J, et al. Ultrafast optical-pump terahertz-probe spectroscopy of the carrier relaxation and recombination dynamics in epitaxial graphene. Nano Lett 2008;8:4248–51.
[28] Jnawali G, Rao Y, Yan H, Heinz TF. Observation of a transient decrease in terahertz conductivity of single-layer graphene induced by ultrafast optical excitation. Nano Lett 2013;13:524–30.
[29] Bao Q, Loh KP. Graphene photonics, plasmonics and broadband optoelectronic devices. ACS Nano 2012;6:3677–94.
[30] Jablan M, Buljan H, Soljacic M. Plasmonics in graphene at infrared frequencies. Phys Rev B 2009;80:245435.
[31] Sensale-Rodriguez B, Yan R, Liu L, et al. Graphene for reconfigurable terahertz optoelectronics. Proc IEEE 2013;101:1705–16.
[32] Withayachumnankul W, Abbott D. Metamaterials in the terahertz regime. IEEE Photon J 2009;1:99–118.
[33] Rahm M, Li JS, Padilla WJ. THz wave modulators: a brief review on different modulation techniques. J Infrared Millim Terahertz Waves 2013;34:1–27.
[34] Zheludev NI, Kivshar YS. From metamaterials to metadevices. Nat Mater 2012;11:917–24.
[35] Zheludev NI. The road ahead for metamaterials. Science 2010;328:582–3.
[36] Zheludev NI, Plum E. Reconfigurable nanomechanical photonic metamaterials. Nat Nanotech 2016;11:16–22.
[37] Jahani S, Jacob Z. All-dielectric metamaterials. Nat Nanotech 2016;11:23–36.
[38] Chen HT, Taylor AJ, Yu N. A review of metasurfaces: physics and applications. Rep Prog Phys 2016;79:076401.
[39] Prinz VY, Naumova EV, Golod SV, Seleznev VA, Bocharov AA, Kubarev VV. Terahertz metamaterials and systems based on rolled-up 3D elements: designs, technological approaches, and properties. Sci Rep 2017;7:43334.
[40] Xie Z, Wang X, Ye J, et al. Spatial terahertz modulator. Sci Rep 2013;3:3347.
[41] Weis P, Garcia-Pomar J, Hoeh M, Reinhard B, Brodyanski A, Rahm M. Spectrally wide-band terahertz wave modulator based on optically tuned graphene. ACS Nano 2012;6:9118–24.
[42] Okada T, Tanaka K. Photo-designed terahertz devices. Sci Rep 2011;1:121.
[43] Zhang B, He T, Shen J, et al. Conjugated polymer-based broadband terahertz wave modulator. Opt Lett 2014;39:6110–3.
[44] Mezzapesa FP, Columbo LL, Rizza C, et al. Photo-generated metamaterials induce modulation of CW terahertz quantum cascade lasers. Sci Rep 2015;5:16207.
[45] Wen QY, Tian W, Mao Q, et al. Graphene based all-optical spatial terahertz modulator. Sci Rep 2014;4:7409.
[46] Deng L, Teng J, Liu H, et al. Direct optical tuning of the terahertz plasmonic response on InSb subwavelength gratings. Adv Opt Mater 2013;1:128–32.
[47] Padilla WJ, Taylor AJ, Highstrete C, Lee M, Averitt RD. Dynamical electric and magnetic metamaterial response at terahertz frequencies. Phys Rev Lett 2006;96:107401.
[48] Chen HT, O'Hara JF, Azad AK, et al. Experimental demonstration of frequency-agile terahertz metamaterials. Nat Photonics 2008;2:295–8.
[49] Kleine-Ostmann T, Dawson P, Pierz K, Hein G, Koch M. Room-temperature operation of an electrically driven terahertz modulator. Appl Phys Lett 2004;84:3555–7.
[50] Chen HT, Padilla WJ, Zide JMO, Gossard AC, Taylor AJ, Averitt RD. Active terahertz metamaterial devices. Nature 2006;444:597–600.
[51] Chen HT, Padilla WJ, Cich MJ, Azad AK, Averitt RD, Taylor AJ. A metamaterial solid-state terahertz phase modulator. Nat Photonics 2009;3:148–51.
[52] Sensale-Rodriguez B, Yan R, Kelly MM, et al. Broadband graphene terahertz modulators enabled by intraband transitions. Nat Commun 2012;3:780.

[53] Sensale Rodriguez B, Yan R, Rafique S, et al. Extraordinary control of terahertz beam reflectance in graphene electro-absorption modulators. Nano Lett 2012;12:4518–22.
[54] Shrekenhamer D, Chen W-C, Padilla WJ. Liquid crystal tunable metamaterial absorber. Phys Rev Lett 2013;110:177403.
[55] Savo S, Shrekenhamer D, Padilla WJ. Liquid crystal metamaterial absorber spatial light modulator for THz applications. Adv Opt Mater 2014;2:275–9.
[56] Chikhi N, Lisitskiy M, Papari G, Tkachenko V, Andreone A. A hybrid tunable THz metadevice using a high birefringence liquid crystal. Sci Rep 2016;6:34536.
[57] Vasic B, Zografopoulos DC, Isic G, Beccherelli R, Gajic R. Electrically tunable terahertz polarization converter based on overcoupled metal-isolator-metal metamaterials infiltrated with liquid crystals. Nanotechnology 2017;28:124002.
[58] Pitchappa P, Manjappa M, Ho CP, Singh R, Singh N, Prakash CL. Active control of electromagnetically induced transparency analog in terahertz MEMS metamaterial. Adv Opt Mater 2016;4:541–7.
[59] Ma F, Lin YS, Zhang X, Lee C. Tunable multiband terahertz metamaterials using a reconfigurable electric split-ring resonator array. Light Sci Appl 2014;3:e171.
[60] Han Z, Kohno K, Fujita H, Hirakawa K, Toshiyoshi H. MEMS reconfigurable metamaterial for terahertz switchable filter and modulator. Opt Express 2014;22:21326–39.
[61] Li J, Shah CM, Withayachumnankul W, et al. Mechanically tunable terahertz metamaterials. Appl Phys Lett 2013;102:121101.
[62] Unlu M, Hashemi MR, Berry CW, Li S, Yang SH, Jarrahi M. Switchable scattering meta-surfaces for broadband terahertz modulation. Sci Rep 2014;4:5708.
[63] Lee SH, Choi M, Kim TT, et al. Switching terahertz waves with gate-controlled active graphene metamaterials. Nat Mater 2012;11:936–41.
[64] Valmorra F, Scalari G, Maissen C, et al. Low-bias active control of terahertz waves by coupling large-area CVD graphene to a terahertz metamaterial. Nano Lett 2013;13:3193–8.
[65] Degl'Innocenti R, Jessop DS, Shah YD, et al. Low-bias THz amplitude modulator based on split-ring resonators and graphene. ACS Nano 2014;8:2548–54.
[66] Liang G, Hu X, Yu X, et al. Integrated terahertz graphene modulator with 100% modulation depth. ACS Photon 2015;2:1559–66.
[67] Degl'Innocenti R, Jessop DS, Sol CWO, et al. Fast modulation of terahertz quantum cascade lasers using graphene loaded plasmonic antennas. ACS Photon 2016;3:464–70.
[68] Jessop DS, Kindness SJ, Xiao L, et al. Graphene based plasmonic terahertz amplitude modulator operating above 100 MHz. Appl Phys Lett 2016;108:17110.
[69] Singh PK, Sonkusale S. High speed terahertz modulator on the chip based on tunable terahertz slow waveguide. Sci Rep 2017;7:40933.
[70] Zhang Y, Qiao S, Liang S, et al. Gbps terahertz external modulator based on a composite metamaterial with a double-channel heterostructure. Nano Lett 2015;15:3501–6.
[71] Mittendorff M, Li S, Murphy TE. Graphene-based waveguide-integrated terahertz modulator. ACS Photon 2017;4:316–21.
[72] Liu PQ, Luxmoore IJ, Mikhailov SA, et al. Highly tunable hybrid metamaterial employing split-ring resonators strongly coupled to graphene surface plasmons. Nat Commun 2015;6:8969.
[73] Low T, Avouris P. Graphene plasmonics for teraherts to mid-infrared applications. ACS Nano 2014;8:1086–101.
[74] Koppens FHL, Chang DE, Garcia de Abajo FJ. Graphene plasmonics: a platform for strong light-matter interactions. Nano Lett 2011;11:3370–7.
[75] Ju L, Geng B, Horng J, et al. Graphene plasmonics for tunable terahertz metamaterials. Nat Nanotech 2011;6:630–4.
[76] Liu PQ, Valmorra F, Maissen C, Faist J. Electrically tunable graphene anti-dot array terahertz plasmonic crystals exhibiting multi-bad resonances. Optica 2015;2:135–40.
[77] Vakil A, Engheta N. Transformation optics using graphene. Science 2011;332:1291–4.
[78] Singh JGR, Liu X, Zhang X, et al. Active control of electromagnetically induced transparency analogue in terahertz metamaterials. Nat Commun 2012;3:1151.
[79] Jadidi MM, Sushkov AB, Myers-Ward RL, et al. Tunable terahertz hybrid metal-graphene plasmons. Nano Lett 2015;15:7099–104.
[80] Shi SF, Zeng B, Han HL, et al. Optimizing broadband terahertz modulation with hybrid graphene metasurface structures. Nano Lett 2015;15:372–7.
[81] Soukoulis CM, Wegener M. Past achievements and future challenges in the development of three-dimensional photonic metamaterials. Nat Photonics 2011;5:523–30.
[82] Zhou J, Chowdhury DR, Zhao R, et al. Terahertz chiral metamaterials with giant and dynamically tunable optical activity. Phys Rev B 2012;86:035448, https://doi.org/10.1103/PhysRevB.86.035448.
[83] Zhang S, Zhou J, Park YS, et al. Photoinduced handedness switching in terahertz chiral metamolecules. Nat Commun 2012;3:942.
[84] Kan T, Isozaki A, Kanda N, et al. Enantiomeric switching of chiral metamaterial for terahertz polarization modulation employing vertically deformable MEMS spirals. Nat Commun 2015;6:8422.
[85] Koenig S, Lopez-Diaz D, Antes J, et al. Wireless sub-THz communication system with high data rate. Nat Photonics 2013;7:977–81.
[86] Suen JY, Fang MT, Denny SP, Lubin PM. Modeling of terabit geostationary terahertz satellite links from globally dry locations. IEEE Trans THz Sci Technol 2015;5:299–313.
[87] Choudhury B, Sonde AR, Jha RM. Terahertz antenna technology for space applications. Singapore, Springer Briefs in electrical and Computer Engineering, 2016.
[88] Bordács S, Kézsmárki I, Szaller D, et al. Chirality of matter shows up via spin excitations. Nat Phys 2012;8:734–8.
[89] Park BC, Kim TH, Sim KI, et al. Terahertz single conductance quantum and topological phase transitions in topological insulator Bi_2Se_3 ultrathin films. Nat Commun 2015;6:6552.
[90] Richter H, Pavlov SG, Semenov AD, et al. Submegahertz frequency stabilization of a terahertz quantum cascade laser to a molecular absorption line. Appl Phys Lett 2010;96:071112.
[91] Ren Y, Hovenier JN, Cui M, et al. Frequency locking of single-mode 3.5-THz quantum cascade lasers using a gas cell. Appl Phys Lett 2012;100:041111.
[92] Ren Y, Hayton DJ, Hovenier JN, et al. Frequency and amplitude stabilized terahertz quantum cascade laser as local oscillator. Appl Phys Lett 2012;101:101111.
[93] Dhillon SS, Vitiello MS, Linfield EH, et al. The 2017 terahertz science and technology roadmap. J Phys D: Appl Phys 2017;50:043001.